ICSV19
Vilnius, Lithuania
July 08-12, 2012

FLUID-STRUCTURE INTERACTION ON THE COMBUSTION INSTABILITY

A. Can Altunlu[1*], Mina Shahi[2*], Artur Pozarlik[*], P.J.M. van der Hoogt[*], J.B.W. Kok[*] and Andre de Boer[*]

**University of Twente, Dept. of Mechanical Engineering, P.O. Box 217, 7500 Enschede, The Netherlands.*
email [1]: a.c.altunlu@utwente.nl, email [2]: m.shahi@utwente.nl.

The multi-domain problem, the limit cycle behaviour of unstable oscillations in the LIMOUSINE model combustor has been investigated by numerical and experimental studies. A strong interaction between the aerodynamics-combustion-acoustic oscillations has been observed during the operation. In this regime, the unsteady heat release by the flame is the acoustic source inducing pressure waves and subsequently the acoustic field acts as a pressure load on the structure. The vibration of the liner walls generates a displacement of the flue gas near the wall inside the combustor which generates an acoustic field proportional to the liner wall acceleration. The two-way interaction between the oscillating pressure load in the fluid and the motion of the structure under the limit cycle oscillation can bring up elevated vibration levels, which accelerates the degradation of liner material at high temperatures. Therefore, fatigue and/or creep lead the failure mechanism. In this paper the time dependent pressures on the liner and corresponding structural velocity amplitudes are calculated by using ANSYS workbench V13.1 software, in which pressure and displacement values have been exchanged between CFD and structural domains transiently creating two-way fluid-structure coupling. The flow of information is sustained between the fluid dynamics and structural dynamics. A validation check has been performed between the numerical pressure and liner velocity results and experimental results. The excitation frequency of the structure in the combustor has been assessed by numerical, analytical and experimental modal analysis in order to distinct the acoustic and structural contribution.

1. Introduction

Since the combustion process generates cyclic stresses and elevated temperature, the structural design of hot components must consider elasticity and plasticity including time dependent creep phenomena. The deformation mechanism, beside cyclic fatigue reversals, can induce creeping in the material at high enough temperatures (homologous temperature) while the stress level kept constant. The lifetime reduction of the hot section components can be accelerated and eventually leaded to failure even for loads less than the material strength.

The pressure variations induced by the fluid flow and the rate of heat release fluctuation due to the flame generate structural vibrations in the gas turbine combustion chamber. The vibration levels can be significantly amplified due to thermo-acoustic instabilities in the system. Depending on the frequency of the acoustic pressure oscillations applied on the structure inner surface, the frequency of the limit cycle and/or the non-linear harmonics can be coupled to the structural eigenfrequencies and can lead to elevated vibrations in resonance. Those strong vibrations may act as an

another acoustic source emitting the acoustic waves to the surrounding fluid and thus additional pressure waves can be formed [1] that can alter the acoustic field in the volume due to this interaction [2]. The acoustic energy not only absorbed by the structural vibrations but also the motion of the walls contribute in dissipation of the energy [3].

2. Methodology

Experimental investigations have been carried out to characterize the structural behaviour of the liner exposed to the combustion process including stable and unstable regimes. The elevated pressure oscillations and the corresponding structural vibrations due to the dynamic combustion and the fluid and structure temperature measurements have been performed in a laboratory-scaled generic combustor test system and the results compared with the fluid-structure interaction numerical analysis. The combustor was heated up gradually and progressed to the desired operating point to prevent possible thermal shocks in the start-up periods. Prior to the full investigation, a stability map has been produced to decompose the unstable and stable operating points and two extreme points (case40180 and case60120) on the envelope has been detailed. The test cases are depicted in Table 1.

Table 1. Combustion test cases

Case Code	Thermal power	Air/fuel ratio	Case Code	Thermal power	Air/fuel ratio
Case40120	40 kW	1.2	Case60120	60 kW	1.2
Case40140	40 kW	1.4	Case60180	60 kW	1.8
Case40180	40 kW	1.8			

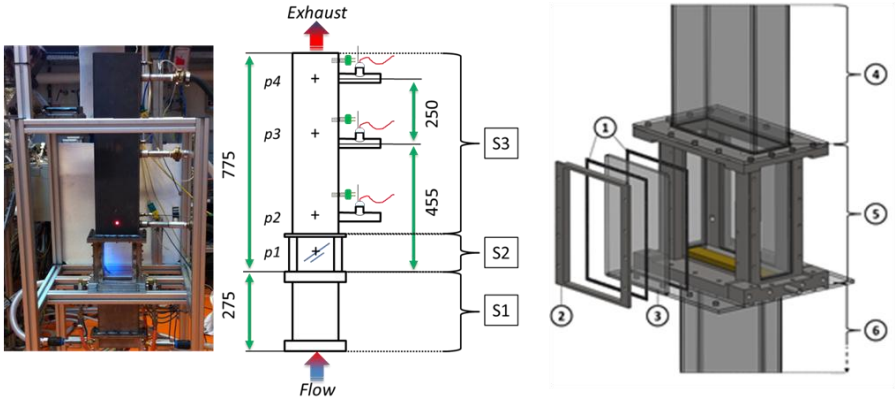

Figure 1. Combustor test system configuration (left) and flame box and specimen assembly (right).

2.1 Experimental combustor system design

The generic combustion test system is depicted in Figure 1 and the geometric dimensions are given in Table 1. In the figure, the letter ‘p’ is the measurement location for the pressure, fluid temperature and the vibration levels.

The combustor has been designed as a Rijke tube configuration consisting of mainly two sections. The upstream section (S1) consists of an air-feeding box, a rectangular duct with a 25x150 mm^2 cross-sectional area and 275 mm long and an equilateral triangular wedge as a flame holder, where methane as the fuel is injected through the holes on the both sides, fixed at the end. The downstream section consists of a flame box (S2) and a rectangular liner (S3). The flame box is surrounded by four quartz glass windows providing an optical access to the flame. Additionally the glass windows can be easily replaced by an intact or a damaged test specimen to investigate the structural dynamics during the operation while visualizing the flame through the side windows. The turbulent flame is technically premixed and flame stabilization takes place on the wedge wake in the combustor test system. The combustor is supported from the bottom of the flame box.

Table 2. Combustor test system dimensions.

Symbol	Section	Dimension [mm]
W_c	Combustor width	158
d_1	Depth of upstream	33
d_2	Depth of downstream	58
B_w	Liner wall thickness	4
B_q	Quarts glass thickness	5
B_s	Specimen thickness	1
W_s	Specimen width	108
L_s	Specimen length	150

2.2 Test specimen configuration and compliance

The test specimens have been laser cut from AISI type 316 steel plate. The material preference has been based on the well-investigated properties and sufficiently enough heat and corrosion resistance for the performed combustion tests. The test specimen material has adequate high temperature strength and creep resistance relatively to the performed test conditions. A third degree polynomial correlation in Eq. (1) is best fitted to the thermal and structural material data [4-7] seen in Table 3 as a function of temperature ranging from 300 – 1200 K. The labels and the units of the material data presented in the table are; Young's modulus (E) [GPa], thermal conductivity (k) [W/m-K], specific heat capacity (c) [kJ/kg-K], yield stress(σ_y) [MPa], coefficient of thermal expansion (α) [m/m-K]. The coefficients (with 95% confidence bounds) of the function, where T is normalized by mean 650 and std 244.9. A comparative deviation of the temperature dependence of the elastic modulus and thermal conductivity for a typical combustor base material nickel-base superalloy Haynes 230 and steel grades are depicted in Figure 2.

$$f(T) = p_1 T^3 + p_2 T^2 + p_3 T + p_4 \qquad (1)$$

Table 3. Coefficient of the material property function.

Coefficients	E	k	c	σ_y	α (*10^{-6})
p_1	- 0.4335	0.05567	4.862	- 9.279	0.08458
p_2	- 2.513	- 0.125	- 10.39	14.85	- 0.3683
p_3	- 19.26	3.661	36.92	- 17.38	1.126
p_4	170.7	19.07	556.5	124.6	17.74

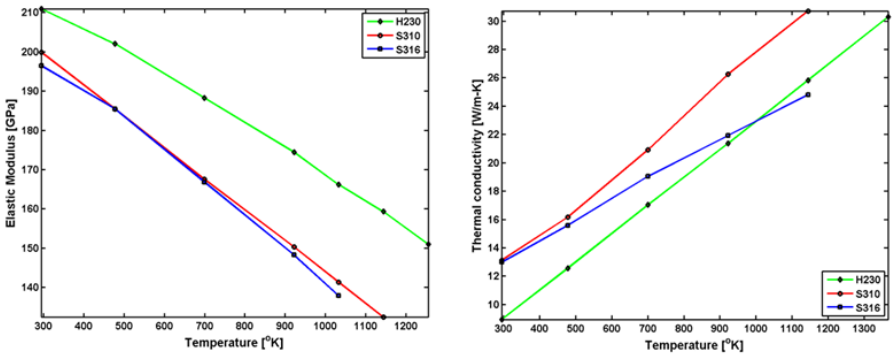

Figure 2. Temperature dependence of material properties.

3. 2-way Fluid structure interaction (FSI) coupling

In the partitioned approach, separate and independent techniques with the appropriate interface boundary conditions are used for the fluid and solid domains. During the two way interaction analysis the CFX and ANSYS software exchange information dynamically every time step, as

shown in Figure 3 (a). Compared to one way interaction, this allows to observe the impact of the wall vibration on the pressure distribution inside the combustion chamber as well as the effect of the modified pressure on the wall vibration. During the 2-way fluid structure interaction (FSI) numerical simulation using ANSYS V13.0 Workbench the data from a steady state solution (CFX fluid flow module A) is fed into the static structural analysis (ANSYS module B) and then to the transient structural (ANSYS module D) and fluid flow (CFX fluid flow module E). A 2-way coupling between the fluid and structure is obtained by linking the modules D and E and then transferring surface loads/displacements across interface. In this way the quantities from the fluid computations are applied directly on the liner and then the new deformed structure is updated in the fluid simulation. This procedure is repeated until a converged solution is obtained, then the calculation will continue in the next time step. This procedure has three levels of iterations which is shown in Figure 3 (b).

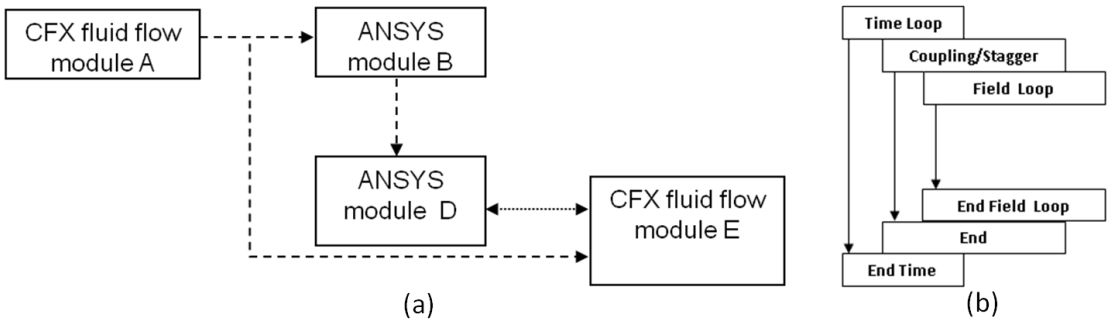

Figure 3. A schematic view of the 2-way fluid structure interaction (FSI) numerical setup (a) and process scheme of 2-way FSI simulation.

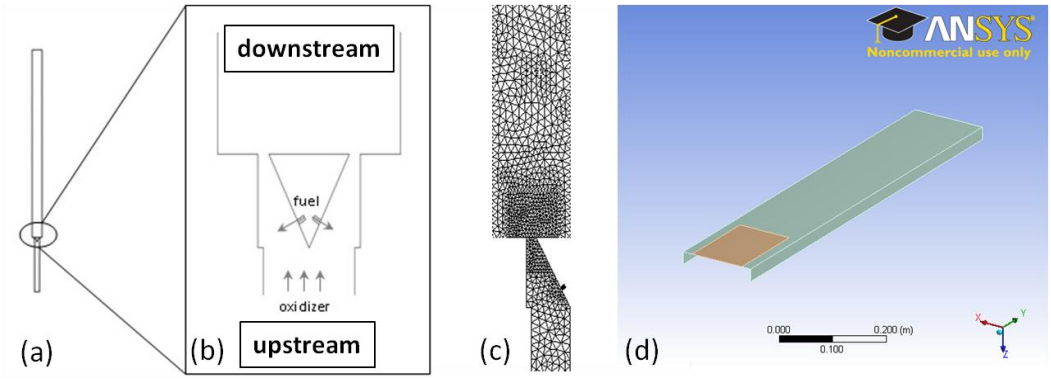

Figure 4. (a) Full combustor, (b) close-up around the wedge, (c) mesh details, (d) FE model of the liner.

3.1 CFX: Computational fluid dynamics (CFD)

In order to reduce the computational effort numerical calculations of the reacting flow inside the combustion chamber are done only for the half part of the geometry, which comprises half of the wedge and is 25 mm wide (Figure 4). The SAS-SST model available in the CFX code is used for the turbulence modelling[8], and the Burning Velocity Model (BVM) for the combustion[9]. A time constant average static pressure is imposed on the outlet. Symmetry boundary conditions are prescribed to the side wall. Except for the walls downstream the wedge the rest are assumed to be adiabatic. Thermal conductivity of those non-adiabatic walls was considered to be constant, the variation with the temperature was neglected. Details about the boundary conditions imposed on the fuel and air inlets are summarized in Table 4. The numerical scheme uses a high resolution advection scheme for spatial and second order backward Euler discretization for time accuracy. Simulations are carried out with a time step of 0.0001 s. At the monitor points the data is stored of the simulations at every time step giving a sampling frequency of 10 kHz, hence the maximum frequency observed is 5 kHz. However only data up to 1 kHz is presented here. A total calculation time of 0.2 s and residual target value of 1e-4 has been achieved.

Table 4. More details about inlet boundary conditions

	B.c	T (k)	Mixture fraction	Reaction progress	Turbulence (intensity)
Air Inlet	Mass flow rate	293	0	0	5%
Fuel inlet	Normal speed	293	1	0	5%

3.2 ANSYS: Computational structural dynamics (CSD)

Because most of the dynamic coupling between the hot fluid and structure occurs in the region downstream of the wedge, in this simulation only the structure downstream of the wedge is considered which is shown in Figure 4 (d). The wall is simplified to three plates forming half of a duct without quartz glass windows or ports for thermocouples and pressure transducer, however intact rectangular plate with 1 mm thickness have inserted into the flame box wall on the place of the windows in order to examine the combustion driven damage mechanisms. A uniform wall temperature equal to 400^{o}C and material properties according to this temperature are used for the analysis. The liner of the test rig was modelled as an elastic material (Shell 63 [9] with 4 mm thickness) with the properties representing hot steel at 400^{o}C which are shown in Table 3 and the corresponding density is 7715 kg/m^3. The total number of 2450 shell elements equally distributed is used for this simulation. Mechanical loads, i.e. pressure and shear are transferred from the CFD domain to structural part at every time step. The clamped boundary condition is implemented at one end. while symmetry condition is used on side edges. The rest of the geometry is allowed to deform freely depending on the dynamic pressure loads. The total calculation real time is 0.2.

Table 5. Calculated acoustic eigenfrequency

Mode	1	2	3
Eigen-Frequency [Hz]	249	747	1247

Table 6. Eigenfrequencies [Hz] of intact combustor T_{room}

Mode	LDV test	Hammer test	FEM
Bending (1st)	125	125	126
Torsional (1st)	534	534	437
Plate (1st)	639	639	633
Bending (2nd)	645	645	532
Plate (2nd)	673	673	671
Plate (3rd)	744	744	750
Torsional (2nd)	764	764	761

3.3 Modal analysis

Acoustic modes calculated with FEM code are presented in Table 5. These three acoustic modes are distinguished in the investigated frequency range. The first acoustic mode represent a half of the acoustic wave in longitudinal direction. The summary of the structural modal analysis and experimental data is shown in Table 6. The experimentally measured frequencies are in agreement with the numerical results except the first torsional and the second bending modes. Since the liner has two L-shaped profiles corner-welded together to have the rectangular cross-section, the welds provides an additional stiffness for those modes that are underestimated compare to the numerical results.

3.4 Acoustic behaviour

Five comparative tests have been carried out to observe the pressure amplitudes between the unstable and the stable combustion (Figure 5). Case6120 has the highest pressure peak among the

unstable cases, case40120 and case40140. Instability also showed harmonics of the first peak with comparably small amplitudes. The temperature of the flue gas induced by the combustion depends on the operating points, thus the limit-cycle oscillation frequency is not fixed but falls within a 5 Hz range. The left bottom and right upper operating points from the stability map envelope (Figure 5) are the extreme cases that have been selected for further investigation: case60120 unstable and case40180 stable.

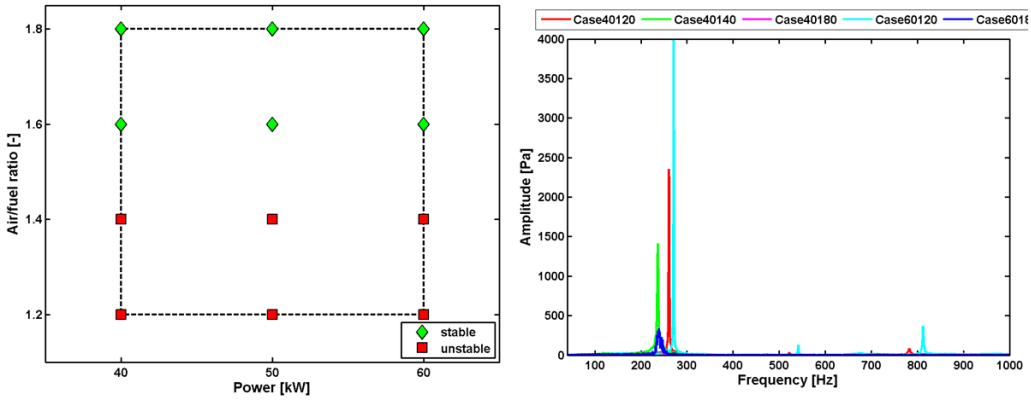

Figure 5. Stability map (left) and pressure spectrum at p4 sensor location (right)

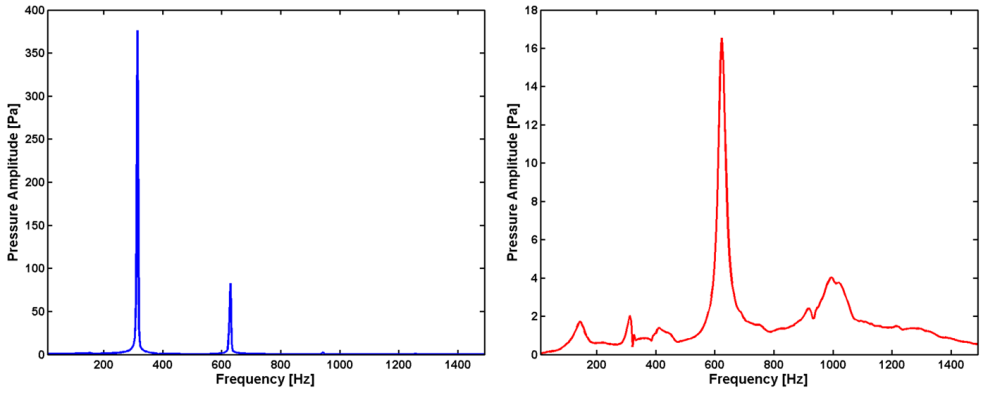

Figure 6. Numerical results for the pressure spectrum of the case6012 (left) and 40180 (right) at p4 location

The FSI numerical results for the pressure spectrums of the unstable and stable cases have been shown in Figure 6. As it can be seen also in Figure 5, for the case60120 in the both graphs two main peaks are clear. However this comparison shows a distinct difference in the magnitude of instability, which is mainly due to over prediction of temperature in the CFD simulation. Furthermore, there are some more limitations for the FSI simulation that potentially restrain the convergence to the experimental results. The experimental measurements have been performed in such a way that the measurement time is sufficiently long to capture the real data, however in the FSI simulations there is physical time limit to reduce the computational cost and this numerical duration is not always sufficient enough to reach the peak amplitude as observed in the experiments. The over prediction of gas temperature can be explained by higher temperature and higher speed of sound and consequently higher acoustic eigenmodes. In the simulation, assuming the liner as an isothermal structure with a constant thermal conductivity may be one of the reasons for this deviation from the experiment. In contrast, the experimental results show an apparent temperature gradient along the liner wall, shown in Figure 7, where the maximum measurable temperature is 500 ^{o}C using a thermographic camera. The complexity on the limit-cycle phenomena can form a combination of a standing and a travelling wave inside the combustor. In Figure 8, the simultaneous pressure measurements at three sensor locations along the combustion liner are depicted in a representative time period. The signal shifting in the time domain is an indication of the combined wave type. This slightly out-of-phase vibration along the liner can impose an additional cyclic bending stresses su-

perimposed to the cyclic stresses caused by the cyclic pressure amplitudes generated inside the combustor.

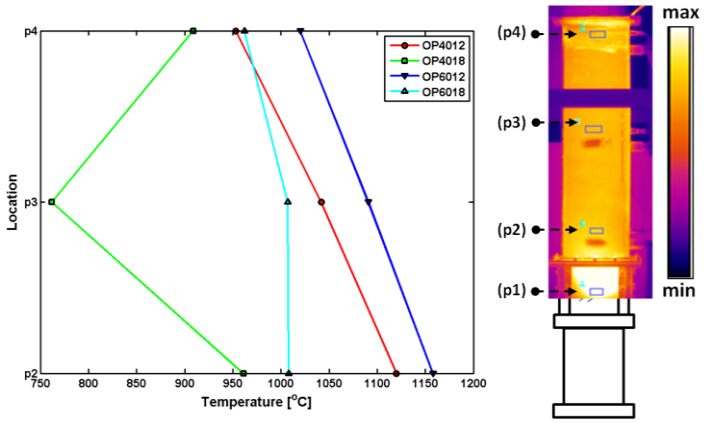

Figure 7. The fluid temperature at sensor locations (left) and the wall temperature profile (right)

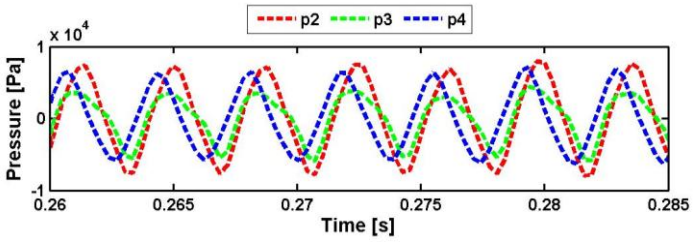

Figure 8. Measured pressure data for Case60120

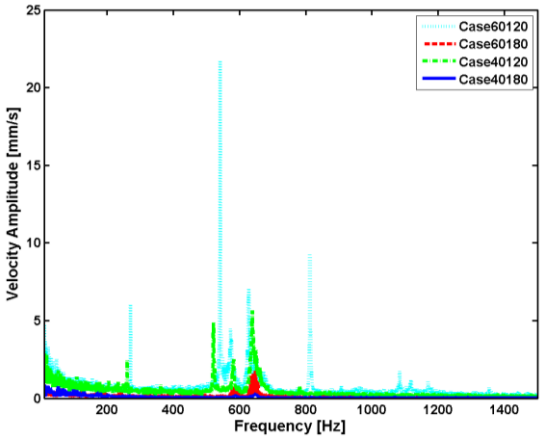

Figure 9. Experimental results for the liner wall velocity

3.5 Structural behaviour

The experimental and numerical results for the wall velocity are compared in Figure 9 and Figure 10 indicating the elevated vibrations levels due to instability. Particularly a closer look to case6012, the numerical data shows that the structure responds mostly to the second acoustic mode which also can be seen in the measured spectrum. However the velocity amplitude predicted by numerical calculation is smaller than the experimental data, which is due to under prediction of pressure amplitude as a driving force.

4. Concluding remarks

The thermo-acoustic instability in the combustion process where the acoustic oscillations, flow perturbations and unsteady heat release forms a feedback mechanism, induces a significant relative motion due to fluid-structure interaction. The unstable combustion leads to the fluttering of

the structure and it can result in a major deterioration or catastrophic failure. Therefore this paper aimed to explore the mechanism of fluid-structure interaction on the LIMOUSINE setup for the stable and unstable regime both numerically and experimentally. However the simplification applied in the numerical approach brought out deviation between the experimental and numerical results. The milestones of the outcome in this research are listed below:

- In all considered cases two distinct frequencies have been observed in pressure spectrums; however comparison shows about15% over prediction in CFD results.
- Calculated and measurement data shows that the structure responds mostly to the second acoustic mode, however there are some peaks in experimental results which are not clear in the CFD data, which could be explained by simplification in the liner and consequently the decrease in the stiffness of the modelled structure.
- An improved FEM for the modal analysis, which contains the welding characteristics present in the structure, can provide more accurate prediction of the modal parameters.
- In comparison to the stable combustion, the unstable cases in the gas turbine engine causes about between %10-%20 increase in the fluid temperature and vibration level scale up by factor 6. The fatigue damage can be sharply promoted with respect to the creep damage and the life-threatening failure mechanisms can tend to alter due to the stability of the combustion.

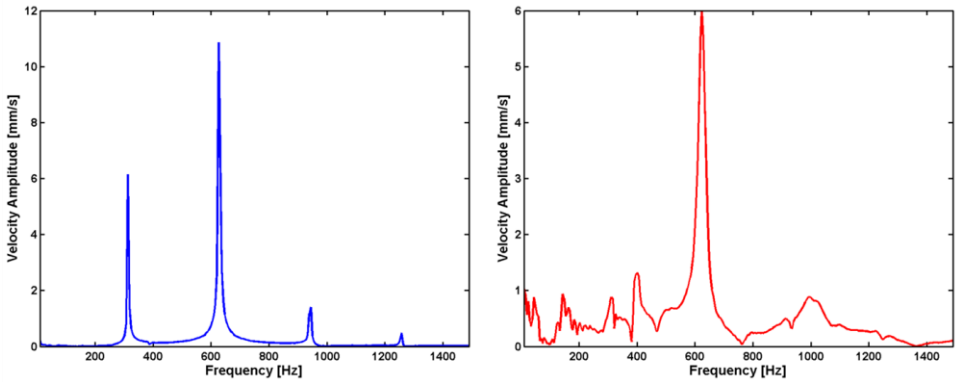

Figure 10. Numerical results for the liner wall velocity of the case60120 (left) and case40180 (right)

Acknowledgement

The authors would like to acknowledge the funding of this research by the EC in the Marie Curie Actions – Networks for Initial Training, under call FP7-PEOPLE-2007-1-1-ITN, Project LIMOUSINE with project number 214905.

REFERENCES

[1] Kaczor, A., & Sygulski, R. (2005). Free vibration analysis of floating plates. 6th International Conference 'ENVIRONMENTAL ENGINEERING, (pp. 774-777). Vilnius.
[2] Davis, R. (2008). Techniques to assess acoustic-structure interaction in liquid rocket engines. Durham: PhD thesis, Duke University.
[3] Pozarlik, A., "Vibro-acoustical instabilities induced by combustion dynamics in gas turbine combustors", (2010), PhD thesis, University of Twente, Enschede, Netherlands.
[4] T. Horie et al., An analytical and experimental study on lifetime predictions for fusion reactor first walls and divertor plates, IAEA-TCM on Lifetime Predictions, Karlsruhe,1985.
[5] Metals Handbook, Ninth Edition, Vol. 2, Properties and Selection: Nonferrous alloys and Pure Metals (American Society for Metals, Metals Park, Ohio, 1979).
[6] D. Peckner and I.M. Bernstein, Handbook of Stainless Steels (McGraw-Hill, New York, 1977).
[7] D.L. Smith, et al. ITER Blanket Shield and Materials Data Base, ITER Documentation Series, No. 29, International Atomic Energy Agency, Vienna (1991).
[8] F.Menter, M Kuntz., R. Bender, A scale-adaptive simulation model for turbulent flow predictions, AIAA Paper 0767, 2003.
[9] ANSYS (2010), Release 11.0 Documentation for ANSYS.